

Quasiclassical trajectory simulation of the kinematically constrained reaction $\text{Ba} + \text{HI} \rightarrow \text{BaI} + \text{H}$

Cite as: J. Chem. Phys. **97**, 6208 (1992); <https://doi.org/10.1063/1.463983>

Submitted: 12 June 1992 . Accepted: 14 July 1992 . Published Online: 04 June 1998

Daqing Zhao, and Richard N. Zare



[View Online](#)



[Export Citation](#)

PHYSICS TODAY
WHITEPAPERS

ADVANCED LIGHT CURE ADHESIVES

Take a closer look at what these
environmentally friendly adhesive
systems can do

[READ NOW](#)

PRESENTED BY
 MASTERBOND
ADHESIVES | SEALANTS | COATINGS



Quasiclassical trajectory simulation of the kinematically constrained reaction $\text{Ba} + \text{HI} \rightarrow \text{BaI} + \text{H}$

Daqing Zhao^{a)} and Richard N. Zare

Department of Chemistry, Stanford University, Stanford, California 94305-5080

(Received 12 June 1992; accepted 14 July 1992)

We report a quasiclassical study of the kinematically constrained reaction $\text{Ba} + \text{HI} \rightarrow \text{BaI} + \text{H}$. A London–Eyring–Polanyi–Sato (LEPS) potential is constructed based on spectroscopic data for BaI, BaH, and HI with its Sato parameters adjusted to reproduce the experimentally determined value of the maximum impact parameter for BaI ($v=0$). The main purpose of the study is to guide future experiments by testing how sensitive different features are to this mass combination. Under the conditions used in the previous Ba+HI crossed-beam experiment, we find that (1) the specific opacity function $P_v(b)$ for a vibrational level v is narrow and overlaps those from neighboring v 's; (2) the most probable impact parameter for reaction producing a given vibrational level decreases as v increases ($v < 12$); (3) the initial orbital angular momentum is mapped onto BaI rotational angular momentum with a spread of $\pm 19\hbar$; (4) the recoil energy has a broad, featureless distribution that is nearly the same for different v levels, and shows no strong correlation with the initial relative velocity, v_{rel} . Product internal-state distributions, recoil angular distributions, and isotope effects are also presented.

I. INTRODUCTION

The reaction



is an example of a kinematically constrained reaction in which the orbital angular momentum $|\mathbf{L}| = \mu v_{\text{rel}} b$ of the reagents appears almost exclusively as the rotational angular momentum of the BaI product. Here μ is the reduced mass of the Ba and HI collision partners, v_{rel} is their initial relative velocity (in the center-of-mass frame), and b is the impact parameter, that is, the distance of closest approach if the two reagents traveled in undeflected, straight-line paths. As first pointed out by Herschbach,¹ the state-resolved product distribution for such a kinematically constrained reaction contains information on the impact-parameter dependence of the reaction. By measuring the amount of BaI product in a vibrational level v and a rotational level J , it is possible to determine the orientation-averaged specific opacity function $P_v(b, v_{\text{rel}})$, where the cross section $\sigma_v(J)$ to form the (v, J) level is related to $P_v(b, v_{\text{rel}})$ by

$$\sigma_v(J) = 2\pi \int \left(\int P_v(b, v_{\text{rel}}) f(v_{\text{rel}}) dv_{\text{rel}} \right) b db. \quad (2)$$

In Eq. (2) $f(v_{\text{rel}})$ is the initial relative velocity distribution of the reagents and the integrations are over all relative velocities and all impact parameters, subject to the constraints of conservation of energy and angular momentum.

This procedure has been applied to the Ba+HI reaction to determine experimentally the form of $P_0(b, v_{\text{rel}})$ from a crossed-beam reaction² and the form of $P_8(b, v_{\text{rel}})$ from a beam-gas reaction.³ In both cases, $P_v(b, v_{\text{rel}})$ was found to be a strongly peaked function of b , where P_0 has a maximum close to 4.5 Å and P_8 close to 2.6 Å.

In this paper we report the simulation of the Ba+HI→BaI+H reaction using a London–Eyring–Polanyi–Sato (LEPS) surface. In this procedure some parameters are fixed by the spectroscopic and thermochemical information about the diatomic reagents and products. Other parameters are adjustable, but these latter were chosen to reproduce most closely the experimentally determined form of $P_0(b, v_{\text{rel}})$. We carry out quasiclassical trajectory calculations^{4,5} on this surface and compare the calculated attributes with those available from experiment. We also derive a number of scattering features that have not yet been measured. Some features arise mainly from the kinematics of this reaction and others are sensitive to the assumed form of the potential-energy surface (PES). The results give us additional confidence in the procedure used to analyze the experiment, help us understand the dynamics of this type of reaction, and suggest possible future studies.

II. THE LEPS POTENTIAL

In the LEPS method^{6–8} with the modification by Kuntz *et al.*,⁹ the potential-energy surface is expressed as

^{a)}Present address: Stanford Magnetic Resonance Laboratory, Stanford University, Stanford, California 94305.

$$\begin{aligned}
 U(r_1, r_2, r_3) = & \frac{Q_1(r_1)}{1+S_1} + \frac{Q_2(r_2)}{1+S_2} + \frac{Q_3(r_3)}{1+S_3} - \left[\left(\frac{J_1(r_1)}{1+S_1} \right)^2 \right. \\
 & + \left(\frac{J_2(r_2)}{1+S_2} \right)^2 + \left(\frac{J_3(r_3)}{1+S_3} \right)^2 \\
 & - \frac{J_1(r_1)J_2(r_2)}{(1+S_1)(1+S_2)} - \frac{J_2(r_2)J_3(r_3)}{(1+S_2)(1+S_3)} \\
 & \left. - \frac{J_3(r_3)J_1(r_1)}{(1+S_3)(1+S_1)} \right]^{1/2}, \quad (3)
 \end{aligned}$$

where r_1 , r_2 , r_3 are the distances r_{AB} , r_{BC} , r_{AC} for the ABC triatomic system, Q_i is the Coulomb integral, and J_i the exchange integral for the diatomic pair i . Assuming Morse and anti-Morse potential functions for the singlet and triplet energies,

$${}^1E_i = {}^1D_i \{1 - \exp[-\beta_i(r_i - r_{ei})]\}^2 - {}^1D_i, \quad (4a)$$

$${}^3E_i = {}^3D_i \{1 + \exp[-\beta_i(r_i - r_{ei})]\}^2 - {}^3D_i, \quad (4b)$$

the Coulomb and exchange integrals are assumed to be given by

$$\frac{Q_i(r_i)}{1+S_i} = ({}^1E_i + {}^3E_i)/2 \quad (5a)$$

and

$$\frac{J_i(r_i)}{1+S_i} = ({}^1E_i - {}^3E_i)/2. \quad (5b)$$

In Eqs. (3), (4), and (5) the parameters are 1D_i , 3D_i , ${}^1\beta_i$, ${}^3\beta_i$, ${}^1r_{ei}$, ${}^3r_{ei}$ and the Sato parameters S_i , where $i=1, 2$, and 3 . The parameters 1D_i , ${}^1\beta_i$, and ${}^1r_{ei}$ are obtained from spectroscopic and thermochemical data for the three different diatomic pairs, BaI, HI, and BaH, where $i=1, 2$, and 3 , respectively.^{10,11} We introduce the additional assumption that ${}^3D_i = {}^1D_i$, ${}^3\beta_i = {}^1\beta_i$, and ${}^3r_{ei} = {}^1r_{ei}$, since little information is available about the triplet states. Consequently, the resulting LEPS surface has only three adjustable parameters, the Sato parameters S_i . They are iteratively adjusted by a trial-and-error method so that the maximum impact parameter forming BaI($v=0$) agrees closely with experiment. $D_0^0(\text{BaI})$ is determined experimentally within ± 2 kcal/mol.¹¹ We also adjust $D_0^0(\text{BaI})$ slightly so that the resulting vibrational distribution is as close as possible to the experimental vibrational distribution. All parameters are listed in Table I.

The LEPS potential given in Eq. (3) favors collinear approach geometries for reaction. It is possible to modify Eq. (3) to favor noncollinear (bent) approach geometries in the manner suggested by Pattengill, Zare, and Jaffe.¹²

TABLE I. Parameters for the BaIH LEPS potential.

i	D_i (eV)	r_{ei} (Å)	β_i (Å ⁻¹)	S_i
BaI	3.24	3.09	0.918	0.19
BaH	1.95	2.23	0.803	0.08
HI	3.05	1.61	1.79	0.17

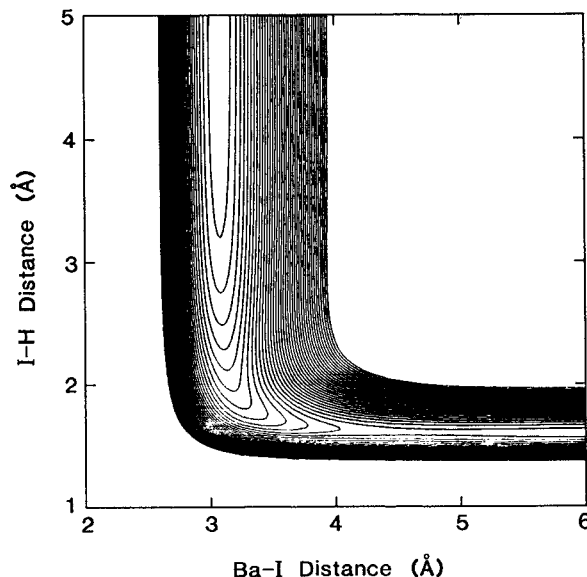


FIG. 1. Collinear cut through the BaIH LEPS surface. The spacing between contours is 0.025 eV (about 0.58 kcal/mol).

We investigated this modification but rejected it because too few trajectories led to BaI products in low v levels compared to the experimental distribution. Even so, the present LEPS surface must be considered only as an approximation. This surface favors unduly collinear approach geometries and ignores the existence of a deep well that corresponds to the bound I-Ba-H species. Moreover, the experimental BaI product distributions show more population in $v=0$ than this potential predicts (see the following).

Figure 1 shows the BaIH LEPS surface, which is seen to have no barrier to reaction. Moreover, the potential is very attractive so that the reaction exoergicity is released early in the entrance valley. Otherwise, this potential is rather featureless. Indeed, the present potential is one of the simplest types of potentials that satisfy the condition that the impact parameters contributing to the formation of BaI($v=0$) be relatively large compared to the BaI equilibrium internuclear distance.

III. QUASICLASSICAL TRAJECTORY CALCULATION

Quasiclassical trajectories (QCT) are calculated in the same manner as described by Pattengill, Zare, and Jaffe.¹² The initial distance between Ba and the HI center of mass is chosen to be 7.5 Å, and the relative velocity distribution is chosen to match experimental conditions² as given in Table II. This corresponds to a distribution with a most probable velocity of 910 m/s and a full width at half max-

TABLE II. Parameters for the velocity distributions where $v_i=0$ for $v_i < v_{0i}$ and $v_i = (v_i - v_{0i})^2 \exp[-(v_i - v_{0i})^2/\alpha_i^2]$ for $v_i > v_{0i}$; see Ref. 11.

i	v_{0i} (m/s)	α_i (m/s)	v_{0i} (m/s)
Ba	242	183	306
HI	771	33	0

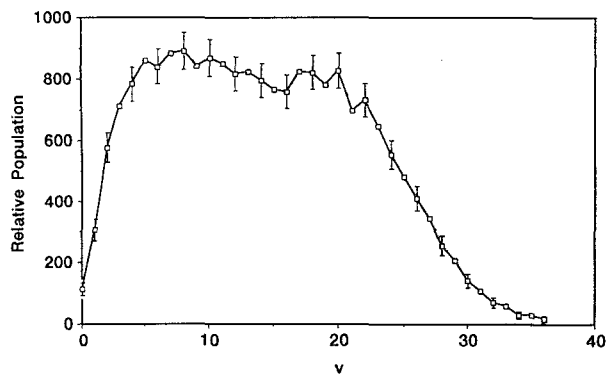


FIG. 2. QCT calculation of $\text{BaI}(v)$ for $\text{Ba} + \text{HI}$. See Table II and text for collision conditions. The error bars represent two standard deviations.

imum of 297 m/s. The impact parameter b is selected randomly from a uniform distribution weighted by $2\pi b$. This choice emphasizes trajectories with large impact parameters. Impact parameters beyond 4.8 \AA are not selected because the reaction probability is clearly zero. The initial rotational state of HI is chosen from a Boltzmann distribution at 20 K, which was the translational temperature of the HI in the N_2 carrier gas. At this temperature, HI is populated up to $J=2$. Since the vibrational frequency is 2300 cm^{-1} , the initial HI vibrational level was restricted to $v=0$. The orientation of HI relative to Ba is selected to be uniformly distributed.

The trajectories are calculated using the six-order Gear hybrid integrator initiated by a Runge-Kutta integrator and Jacobian coordinates are used in the simulation.¹² The step size of integration is 0.2 fs and a test simulation at a 0.1 fs step size confirms that the trajectories are converged.

Trajectories were integrated until one of the three atoms was separated from the other two by 10 \AA . Under these conditions, the only reaction products are BaI and H, i.e., no $\text{BaH} + \text{I}$ occurs. We found that 69% of the trajectories result in reaction. If b_{max} is chosen as 4.3 \AA then 86% of the trajectories are reactive. The total opacity function closely approximates a step-function model. At first glance it might be thought that we would obtain excellent statistics for the formation of the $\text{BaI}(v=0)$ product from $\text{Ba} + \text{HI}$, but fewer than 0.4% of the trajectories yield this reaction product. Most results are based on sorting the attributes of 30 000 trajectories.

A. Product internal-state distribution

Figure 2 presents the BaI vibrational distribution. The bell-shaped distribution agrees qualitatively with the distribution obtained for the beam-beam experiment² but the low- v products are too few and the peak of the distribution is too flat. The apparent structure is a measure of the "noise" in our statistics. We found that the vibrational distribution is very sensitive to $D_0^0(\text{BaI})$. When $D_0^0(\text{BaI})$ is chosen to be 78 kcal/mol the most probable v is 15, whereas when $D_0^0(\text{BaI})$ is 75 kcal/mol the most probable v is only 9. We also found that if the most probable value of the initial relative velocity distribution is shifted from 910

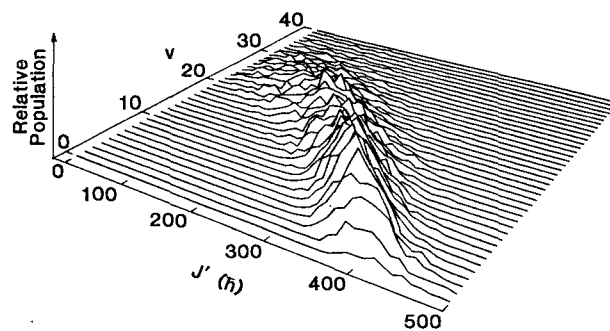


FIG. 3. QCT calculation of the distribution of $\text{BaI}(v, J)$ for $\text{Ba} + \text{HI}$. See Table II and text for collision conditions.

m/s to 1180 m/s, the most probable vibrational level is shifted from 9 to 3 and the full width at half maximum of the distribution is increased from 23 to 35 vibrational levels.

Figure 3 shows the rotational distribution associated with each vibrational state of the BaI product. Several distinctive features are apparent: (1) each vibrational level, especially for $0 < v < 15$, has a "smooth," bell-shaped rotational distribution characterized by a narrow width; (2) the maximum J value decreases with increasing v ; (3) the most probable J value for $\text{BaI}(v=0)$ is about 470; (4) the width of the rotational distribution grows with increasing v , especially for $v > 15$. Once again, noise resulting from too few trajectories in each vibrational level introduces fluctuations that are not believed to be real. The general features of the rotational distribution agree closely with what is known experimentally for $\text{BaI}(v=0)$ (Ref. 2) and $\text{BaI}(v=8)$ (Ref. 3). At higher initial relative velocities the most probable J is increased by about $45\hbar$ and the full width at half maximum is also increased; however, statistical scatter prevents us from quantifying its magnitude.

It is interesting to examine whether certain initial velocities lead preferentially to specific product vibrational states. Figure 4 shows the results of this investigation in which we have plotted the $\text{BaI}(v)$ distribution against ini-

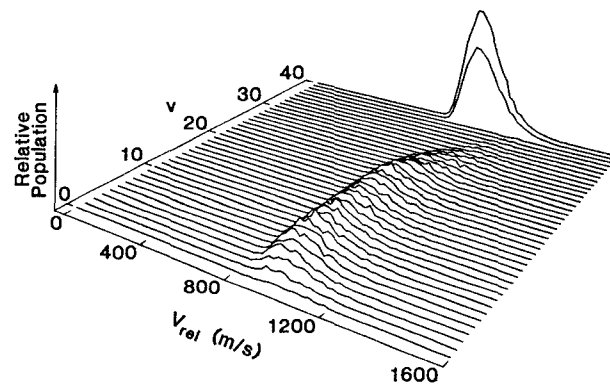


FIG. 4. $\text{BaI}(v)$ versus v_{rel} for $\text{Ba} + \text{HI}$. The relative initial velocity distribution is shown at the extreme top of this figure. Next to it is the distribution of relative velocities that lead to reaction. See Table II and text for collision conditions.

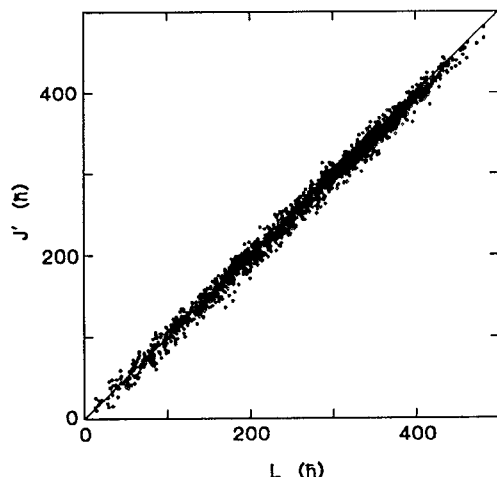


FIG. 5. BaI (all v , J) versus the initial orbital angular momentum L for Ba + HI. See Table II and text for collision conditions.

tial velocity. The initial velocity distribution is shown at the top of Fig. 4 along with the distribution of initial velocities that lead to reaction. We note that there is no velocity discrimination in reactivity, i.e., the two distributions at the top of Fig. 4 have similar shapes. We also find that higher initial velocities result in BaI products with either high v or low v ; consequently, lower initial velocities preferentially populate BaI products with a medium value of vibrational levels.

B. Kinematic features

For the Ba + HI reaction, the mass combination causes the orbital angular momentum of the reagents to be channeled into rotational angular momentum of the BaI product. In the limit of complete kinematic constraint, $|\mathbf{L}|$, which is equal to $\mu v_{\text{rel}} b$, should be mapped directly into the rotational quantum number J of the BaI product. We have tested this relation in Fig. 5, which plots J versus L . It is seen that kinematics strongly constrain this relationship throughout the range of L values to be $J = L \pm 19$ (2σ). Further inspection indicates that J is somewhat smaller than L for large J values. This behavior differs from the result obtained using a collinear model,¹³ which gives almost exactly $J = L$. Our model assumes a linear minimum energy path, but not necessarily all collisions are restricted to be linear. Because the width is about the same for all J values, the spread in the low- J values could be comparable to J . Thus, for low v values characterized by J distributions peaking above $300\hbar$ essentially all the orbital angular momentum of the reagents appears in product rotation. Hence, the separating products BaI(low v) + H carry away little angular momentum. This finding, however, can be misleading in that for BaI products with low v , the J distribution has a width that is only a few times larger than the spread of $\pm 19\hbar$ (2σ). This fact limits our ability to relate the product J distribution to the distribution of impact parameters responsible for producing BaI(low v).

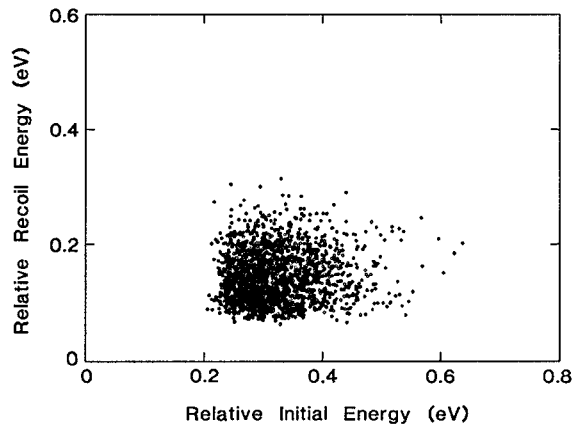


FIG. 6. Product recoil energy versus initial relative collision energy for Ba + HI. See Table II and text for collision conditions.

We have also examined how the recoil energy of the products is related to the initial relative energy of the reagents (see Fig. 6). We find that the BaI product has a recoil energy that exceeds 0.07 eV (1.6 kcal/mol) but seldom is greater than 0.25 eV (~ 6 kcal/mol). The exoergicity of reaction is about 5 kcal/mol. Moreover, within these limits no correlation exists between the initial relative energy and the product recoil energy. Hence, to a first approximation the products have a constant distribution of recoil velocities independent of the initial relative velocity.

It might be wondered whether this behavior also implies that the recoil energy of the products is independent of the vibrational level of BaI. Figure 7 shows that this is approximately true. We also plot in Fig. 7 the total recoil energy distribution, which is compared to the initial relative collision energy distribution. Figure 7 shows that the former is much smaller than the latter. In Fig. 7, there appears to be some bimodal behavior in the recoil energies for a vibrational level that is, for a collision resulting in BaI(v), either higher or lower recoil energies are favored over intermediate ones. This bimodality is more obvious for higher v 's and lies outside of statistical scatter. The

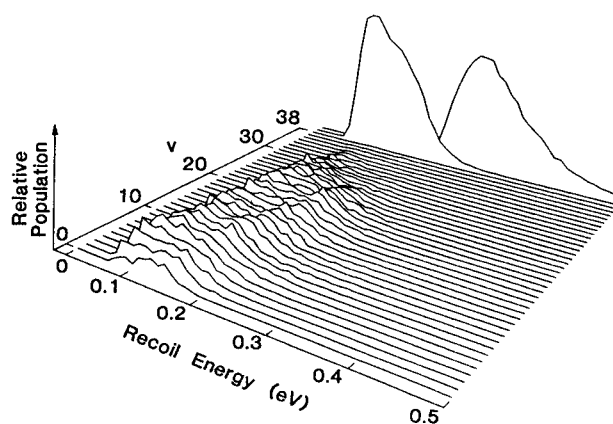


FIG. 7. Product recoil energy versus the BaI vibrational level v . The initial relative energy is plotted on the extreme top of the figure and the total recoil energy distribution is plotted next to it.

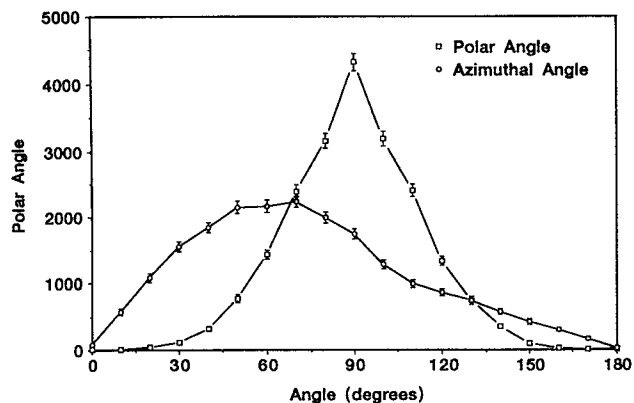


FIG. 8. H-atom angular distribution for $\text{Ba} + \text{HI}$. See text for definitions of polar and azimuthal angles and Table II for collision conditions. The error bars represent two standard deviations.

origin of this bimodality appears to be complex and cannot be described as a simple dependence on the initial phase of the HI oscillator. Inspection of one hundred random trajectories that led to reaction shows that the vibrational phase of the HI moiety at the transition state correlates with product recoil energy.

Note that this model predicts no preference for “zero” recoil energy; this can be viewed as a kinematic consequence of the difficulty in removing all the energy from the light H atom to the heavy Ba and I atoms. Clearly, most of the relative energy between the two heavy atoms Ba and I becomes channeled into internal energy of the BaI product. We examined the recoil energy distribution for a particular product vibrational level, specifically, $\text{BaI}(v=20)$. We found that the product recoil energy was essentially uncorrelated with reagent relative velocity, but the product recoil energy increases with a decrease in either the impact parameter or the rotational angular momentum of the $\text{BaI}(v=20)$ product.

The kinematics also control the form of the H-atom angular distributions. Figure 8 presents the H-atom recoil probability as a function of the angle measured from L (polar angle) and as a function of the angle measured from the vector from Ba to the center of mass of HI (azimuthal angle). We find that the H-atom angular distribution is primarily in the plane defined by the \mathbf{v}_{rel} vector and the position vector connecting the center of mass of HI to the Ba atom. We also see that there is a slight preference for forward scattering (in the direction of the Ba atom to the center of mass of HI). More detailed analysis reveals that collisions with small impact parameters contribute preferentially to scattering in the forward direction, whereas large impact parameters contribute to the backward direction. This behavior is a consequence of the preference for collinear geometry leading to reaction and the smallness of the HI moment of inertia, which allows the HI molecule to reorient during a reactive collision. The backward scattering of collisions at large impact parameters (and hence large L values) also explains the fact that J values are likely to be smaller than L values. Another consequence of

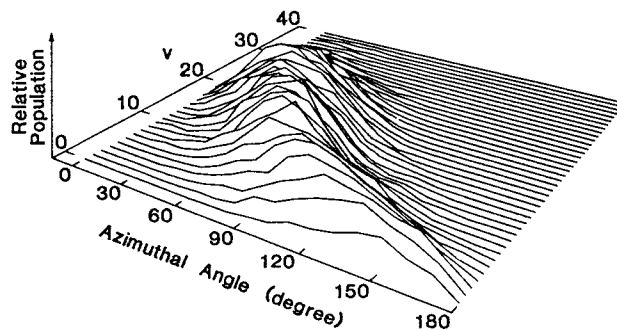


FIG. 9. QCT calculation of $\text{BaI}(v)$ versus H-BaI recoil azimuthal angle. See Table II and text for collision conditions.

this behavior is that the angular distribution changes from backward scattered for $\text{BaI}(\text{low } v)$ to forward scattered for $\text{BaI}(\text{high } v)$, as shown in Fig. 9. In addition, it is also found that recoil energies do not depend on the azimuthal angle, although they increase slightly for either small ($< 30^\circ$) or large ($> 150^\circ$) polar angles, indicating that recoil energies remain about the same for either backward or forward scattered reactions, but increase slightly for out-of-plane scattering.

C. Specific opacity function, $P_v(b)$

Figure 10 presents a plot of the specific opacity function integrated over the relative velocity distribution as a function of the vibrational level v . We see that this simple potential predicts that $P_v(b)$ has a maximum value that decreases with increasing v . Moreover, for low vibrational levels $P_v(b)$ is a narrow distribution whose width appears to change slowly with v until $v \approx 12$ at which point the width increases with increasing v . Also shown in Fig. 10 is the total opacity function

$$P(b) = \sum_v P_v(b). \quad (6)$$

We find that $P(b)$ has the familiar shape of a Heavyside function, being nearly constant for $b < b_{\text{max}}$ and dropping

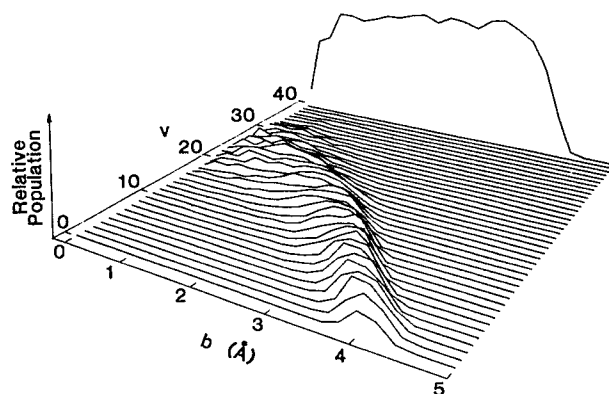


FIG. 10. QCT calculation of $P_v(b)$ versus b for $\text{Ba} + \text{HI}$ at collision conditions given in the text and in Table II. Also shown is the total opacity function $P(b)$.

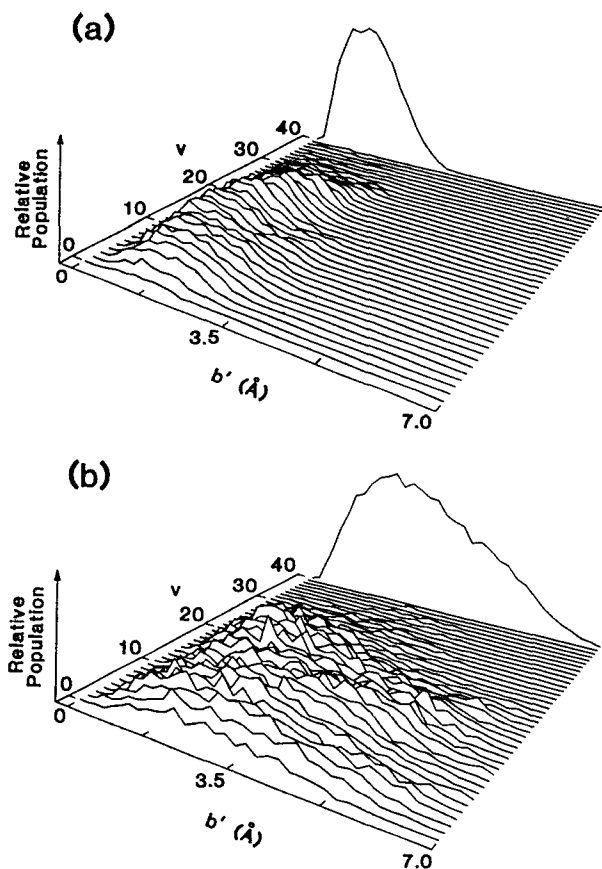


FIG. 11. QCT calculation of the H-BaI recoil impact parameter distribution for (a) Ba+HI and (b) Ba+DI. See Table II and text for collision conditions.

rapidly to zero for $b > b_{\max}$. Thus, this system shows a nested distribution of tree rings so that only certain narrow impact parameter ranges yield a particular BaI(v) product for $v < 12$. We also note that these ranges overlap to some extent from v to $v+1$, etc. Finally, the value of b_{\max} for $P(b)$ is actually somewhat larger (about 0.2 Å) than the value of b_{\max} for $P_0(b)$. This result is surprising and indicates that the tree-ring model provides a good but not complete picture of the decomposition of $P(b)$ into different $P_v(b)$. We also analyzed the average impact parameter for $v=0$ and found that it decreases as relative velocity increases. This is the basis for the “sliding truncated Gaussian” fitting function for the determination of $P_0(b, v_{\text{rel}})$ from the experimentally measured rotational distribution BaI($v=0, J$).²

Figure 11(a) presents a plot of the recoil impact parameter b' for the separating BaI and H products as a function of the vibrational level of the BaI product. In contrast to Fig. 10, this distribution is broad and ranges from about 0.3 to 3.5 Å; moreover, it looks similar for all v values. Hence, the exit channel is not narrow or restricted.

D. Isotope effects

Using the same PES we have investigated the scattering dynamics for Ba+DI→BaI+D for the same initial

conditions as Ba+HI→BaI+H. Compared to Ba+HI, we find that (1) the BaI vibrational distribution is colder by about 5 quanta and falls more rapidly at high v ; (2) the rotational distribution is colder by about 40 quanta; (3) $J \simeq L \pm 31$ (2σ) so that the mapping of initial angular momentum into product rotation is degraded by about 30% which occurs more prominently at high L values, for which J is likely to be smaller than L ; (4) the angular distribution of the products is almost the same; (5) the product recoil energy distribution is nearly the same with the reaction of Ba+DI having a slightly larger recoil energy; (6) the opacity function for BaI($v=0$) peaks at slightly smaller values of b ; (7) the recoil impact parameter distribution broadens by approximately a factor of 2 [see Fig. 11(b)] which indicates that the increase of recoil angular momentum is attributed mainly to the increase in recoil impact parameter rather than to the recoil velocity. Most of these results reflect the change in reduced mass from $\mu_{\text{Ba-HI}} = 66.4$ to $\mu_{\text{Ba-DI}} = 62.3$. It is interesting to note, however, that the recoil impact parameter distribution shows an isotope effect as large as a factor of 2 which reflects the change from $\mu_{\text{H-BaI}} = 1.0$ to $\mu_{\text{D-BaI}} = 2.0$, whereas the corresponding angular distributions remain nearly unchanged.

E. Concluding Remarks

The reaction Ba+HI→BaI+H is the most kinematically constrained system of the type $H+H'L \rightarrow HH'+L$ because Ba and I are the heaviest (nonradioactive) and H the lightest elements in their respective groups in the periodic table. Consequently, this reaction serves as the prototypical example for understanding the nature of the $H+H'L$ kinematic constraint in $A+BC$ bimolecular reactions. The heavy Ba and I atoms, unfortunately, also make *ab initio* calculations of the BaIH PES extremely difficult and no reliable surface is presently available. We used instead a simple approximation—a LEPS surface—constructed to reproduce a few features previously determined from crossed-beam studies of this reaction.² We then carried out quasiclassical trajectory calculations on this LEPS surface so that a number of dynamical features could be investigated.

The present simulation of the Ba+HI reaction system agrees well, in general, with what is experimentally known. In addition, the simulation suggests some characteristics, such as the distribution of recoil velocities, the tree-ring-like nature of the specific opacity function, $P_v(b)$, and the angular distribution of the products, which may guide future experimental studies. Because of the lack of flexibility of the LEPS potential form, we have no reason to believe that the model offers a complete or faithful description of all features of the Ba+HI reaction dynamics. The purpose of this study, however, is to provide results that can motivate and assist parallel experimental studies now in progress.

ACKNOWLEDGMENT

This work was supported by the U.S. National Science Foundation under Grant No. NSF CHE 89-21198.

- ¹D. R. Herschbach, *Adv. Chem. Phys.* **10**, 319 (1966).
²C. A. Leach, A. A. Tsekouras, P. H. Vaccaro, R. N. Zare, and D. Zhao, *Faraday Discuss. Chem. Soc.* **91**, 183 (1991); D. Zhao, Ph.D. thesis, Stanford University, 1991; P. H. Vaccaro, A. A. Tsekouras, D. Zhao, C. A. Leach, and R. N. Zare, *J. Chem. Phys.* **96**, 2786 (1992).
³C. Noda, J. S. McKillop, M. A. Johnson, J. R. Waldeck, and R. N. Zare, *J. Chem. Phys.* **85**, 856 (1986).
⁴M. Karplus, R. N. Porter, and R. D. Sharma, *J. Chem. Phys.* **43**, 3259 (1965).
⁵D. G. Truhlar and J. T. Muckerman, in *Atom-Molecular Collision Theory: A Guide for the Experimentalist*, edited by R. B. Bernstein (Plenum, New York, 1979).
⁶W. Heitler and F. London, *Z. Phys.* **44**, 455 (1927).
⁷H. Eyring and M. Polanyi, *Z. Phys. Chem. B* **12**, 279 (1931).
⁸S. Sato, *J. Chem. Phys.* **23**, 592, 2465 (1952).
⁹P. J. Kuntz, E. M. Nemeth, J. C. Polanyi, S. D. Rosner, and C. E. Young, *J. Chem. Phys.* **44**, 1168 (1966).
¹⁰K. P. Huber and G. Herzberg, *Molecular Spectra and Molecular Structure. IV. Constants of Diatomic Molecules* (Van Nostrand, New York, 1979).
¹¹P. H. Vaccaro, D. Zhao, A. A. Tsekouras, C. A. Leach, W. E. Ernst, and R. N. Zare, *J. Chem. Phys.* **93**, 8544 (1990).
¹²M. D. Pattengill, R. N. Zare, and R. L. Jaffe, *J. Phys. Chem.* **91**, 5489 (1987).
¹³R. D. Levine and R. B. Bernstein, *Molecular Reaction Dynamics and Chemical Reactivity* (Oxford, New York, 1987).